Paleomagnetic, anisotropy of magnetic susceptibility, and geochronologic data from the Buena Vista intrusion, north-central New Mexico

M. S. Petronis, G. Castillo, J. Lindline, J. Zebrowski, W. McCarthy, D. Lemen, and W. McIntosh

2015, pp. 193-204. https://doi.org/10.56577/FFC-66.193

in:

Guidebook 66 - Geology of the Las Vegas Area, Lindline, Jennifer; Petronis, Michael; Zebrowski, Joseph, New Mexico Geological Society 66th Annual Fall Field Conference Guidebook, 312 p. https://doi.org/10.56577/FFC-66

This page is intentionally left blank to maintain order of facing pages.

PALEOMAGNETIC, ANISOTROPY OF MAGNETIC SUSCEPTIBILITY, AND GEOCHRONOLOGIC DATA FROM THE BUENA VISTA INTRUSION, NORTH-CENTRAL NEW MEXICO

M.S. PETRONIS[1], G. CASTILLO[1], J. LINDLINE[1], J. ZEBROWSKI[1], W. McCARTHY[2], D. LEMEN[1], AND W.C. McINTOSH[3]

[1] Enviromental Geology, Natural Resource Management Department, New Mexico Highlands University, Las Vegas, NM, mspetro@nmhu.edu
[2] Irvine Building, University of St Andrews, St Andrews, Fife, Scotland, UK
[3] New Mexico Bureau of Geology & Mineral Resources, New Mexico Institute of Mining and Technology, Socorro, NM

ABSTRACT—The Buena Vista intrusion outcrops on the eastern side of the Sangre de Cristo Mountains near the transition between the Rocky Mountains and the Great Plains. Along the five kilometer strike of the intrusion, at least three compositionally distinct phases occur. These include a marginal augite porphyritic basalt, a main-phase hornblende gabbro, and a central plagioclase-rich (tourmaline anorthosite) phase. In order to assess the emplacement mode, along-strike variation in emplacement style and/or deformation, and the absolute age of emplacement, we conducted detailed rock magnetic, paleomagnetic, anisotropy of magnetic susceptibility (AMS), and $^{40}Ar/^{39}Ar$ age determinations. Rock magnetic experiments reveal that the primary magnetic phase is a cubic, Fe-Ti oxide phase (titanomagnetite) of a pseudosingle domain to multi-domain grain size with low to moderate Ti substitution. Paleomagnetic data from thirteen of the eighteen sites collected yield a dominantly single component reverse polarity magnetization that is clockwise discordant to the mid-Miocene expected direction. AMS data from fifteen of eighteen sites yield remarkably consistent results along strike of the dike, characterized by well-defined oblate susceptibility ellipsoids with magnetic foliation planes that strike parallel to the trend of the dike and K1 magnetic lineations that trend south-southwest with a low plunge (<30°). Four of the five new $^{40}Ar/^{39}Ar$ age determinations yield generally well-defined plateau or isochron ages that range in age from 14.71 Ma to 14.20 Ma. One sample yields a disturbed age spectra for which we did not assign an age. We postulate that the region east of the Sangre de Cristo range front, at this latitude, experienced a modest amount of clockwise vertical axis rotation and that magma emplacement occurred with flow sub-horizontally from the north-northeast to the south-southwest. The Buena Vista intrusion is part of, until now, a previously unrecognized suite of igneous intrusions that were emplaced during the middle Miocene that we define as the Las Vegas Igneous Province.

INTRODUCTION

The Buena Vista intrusion is located southwest of the Ocate Volcanic field in northern-central New Mexico, north of the city of Las Vegas at the transition between the southern Sangre de Cristo Mountains and the Great Plains (Fig. 1). The Buena Vista igneous intrusion is named for the village of Buena Vista (Sp. *pleasant view*) and it is the longest of a suite of northeast-trending dikes in the region. The intrusion is roughly 10 m thick and extends nearly continuously for approximately 5 km. It intrudes the Carlile Shale in the north and the Niobrara Formation in the south. The main phase of the Buena Vista intrusion cross-cuts an augite-porphyritic basaltic dike that outcrops along Arroyo de la Jara and two unnamed drainages near the middle and southern part of the main intrusion (Fig. 2).

The Buena Vista intrusion is a zoned and composite mafic dike. The main phases consist of augite + plagioclase + Fe-Ti oxides ± hornblende in a plagioclase framework. Augite + plagioclase occur as 1–3 mm long single phenocrysts and as agglomerocrysts. A sub-vertically oriented plagioclase-rich phase (anorthosite) occurs near the northern part of the intrusion and ranges from more than 1 m to less than a few centimeters in width. At the surface, the contact between the hornblende gabbro and central anorthosite is curvilinear, suggesting that both were molten contemporaneously. The anorthosite displays a cumulate texture, consisting of closely spaced plagioclase laths with up to 8% emerald green euhedral tourmaline crystals, displaying spectacular zoning in thin section, similar to those at the contact zone. Here, we report the results from a detailed geophysical study of the Buena Vista intrusion, which provides insight into late Cenozoic magmatism east of the Sangre de Cristo Mountains in northern New Mexico. The research goals were to establish the emplacement mode using paleomagnetic and AMS data and to constrain the age of emplacement via $^{40}Ar/^{39}Ar$ age determinations.

ANALYTICAL METHODS

Field Methods

Eight to ten drill core samples were collected at eighteen sites along the strike of the intrusion using a modified Echo 280E gasoline powered drill with a non-magnetic diamond tip drill bit. All samples were oriented using a magnetic and, when possible, a sun compass. At each site, independent core samples were drilled along the margins and/or across the center of the intrusion with the total number of samples collected at each site dependent upon the level of exposure. At twelve sites, samples were collected from paired margins in order to determine a unique magma flow direction based on the AMS techniques as outlined in Tauxe et al. (1998). In total, we have defined unique flow directions from four paired margins in the main phase hornblende gabbro and one paired margin from the central tourmaline anorthosite. Hand specimens were collected for $^{40}Ar/^{39}Ar$ age determinations and for thin section analysis. Field mapping and structural observations

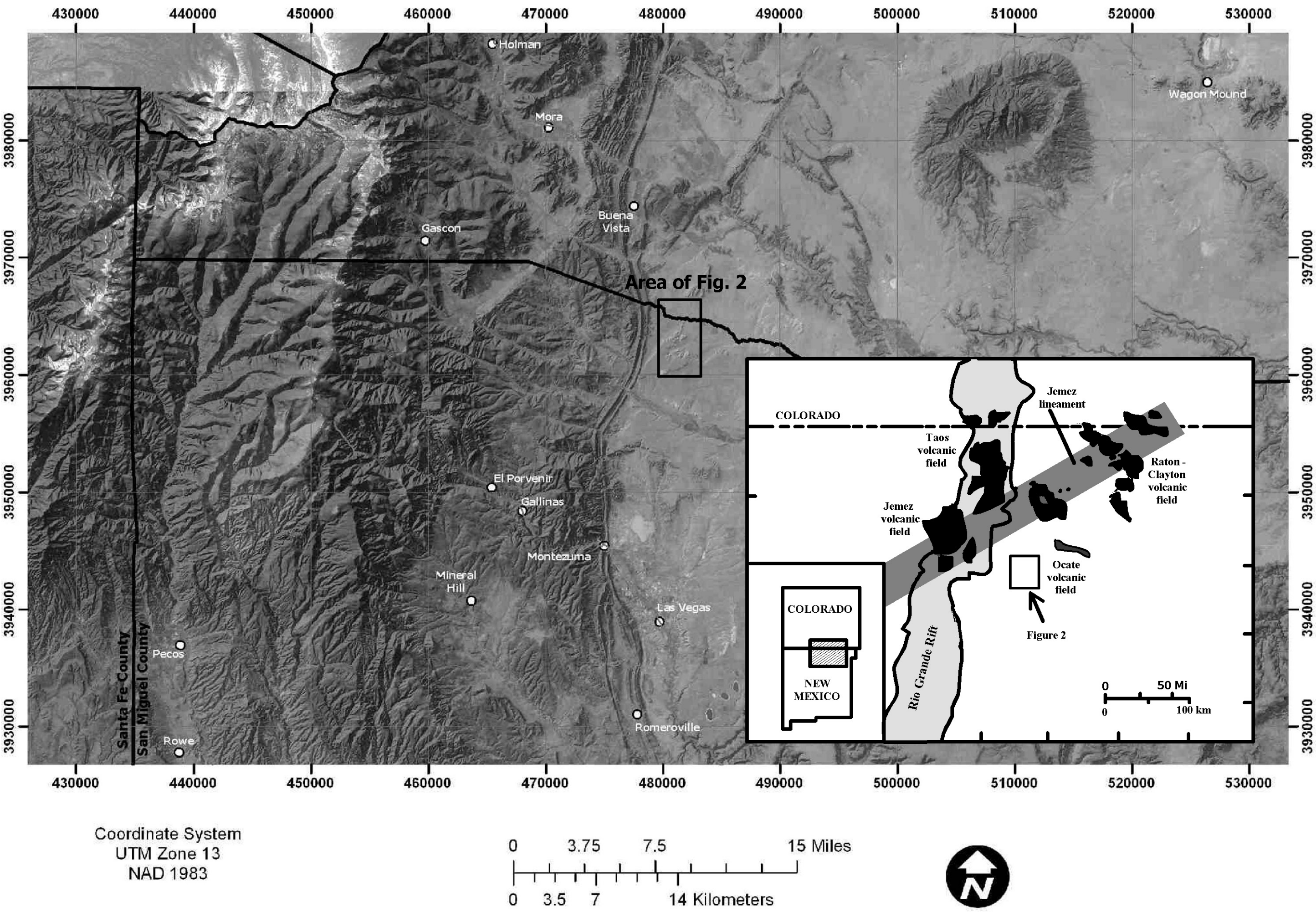

FIGURE 1. Digital elevation model of the region east of the Sangre de Cristo Mountains. The Buena Vista intrusion (noted as Area of Fig. 2) is located at the transition between the Great Plains to the east and the Rocky Mountains to the west. Inset map: Location of the Buena Vista intrusion in north-central New Mexico (modified from Olmstead and McIntosh 2004).

were used to identify kinematic indicators to aid with interpreting the magma flow patterns as well as define relative age relationship between the intrusion segments. All core samples were cut into 2.2 cm by 2.5 cm right cylinder specimens, using a diamond-tipped, non-magnetic saw blade with up to three specimens per sample obtained at New Mexico Highlands University's Rock Processing laboratory.

Paleomagnetic Methods

Remanent magnetizations of all samples were measured using an AGICO JR6A dual-speed spinner magnetometer at the New Mexico Highlands University Paleomagnetic-Rock Magnetism laboratory. Specimens were progressively alternating field (AF) demagnetized, typically in 15 to 30 steps, to a maximum field of 120 mT using a ASC Scientific D-TECH 2000 AF-demagnetizer. Samples with high coercivity were treated with thermal demagnetization (TH) up to a maximum of 630°C, yet with most samples being fully demagnetized by 580°C. Thermal demagnetization experiments on replicate specimens, to compare with AF behavior, were conducted with an ASC Scientific TD48 thermal demagnetizer. Principal component analysis (PCA; Kirschvink, 1980) was used to determine the best-fit line through selected demagnetization data points for each sample (Table 1). For most samples, a single line could be fit to the demagnetization data points. Best-fit magnetization vectors involved 5 to 18 data points, but as few as 3 to as many as 25 were used. Magnetization vectors with maximum angular deviation values greater than 5° were not included in site mean calculations. For less than 10% of the demagnetization results, it was necessary to anchor the magnetization vector to the origin. Individual sample directions were considered outliers and rejected from the site mean calculation if the angular distance between the sample direction and the estimated site mean was greater than 18°.

Anisotropy of Magnetic Susceptibility Methods

Anisotropy of magnetic susceptibility (AMS) measurements of a rock specimen yields an ellipsoid of magnetic susceptibility (K) defined by the length and orientation of its three principal axes, K1 ≥ K2 ≥ K3, which are the three eigenvectors of the susceptibility tensor (Tarling and Hrouda, 1993). The long axis of the magnetic susceptibility ellipsoid, K1, defines the magnetic lineation, while the short axis, K3, defines the normal to the magnetic foliation plane (K1-K2). The bulk magnetic susceptibility (Km) is the arithmetic mean of the principal axes K1, K2 and K3. In addition, the AMS technique defines the degree of magnitude of the linear (L = K1/K2) and planar (F = K2/K3) fabric components. The technique also quantifies the corrected degree of anisotropy, $Pj=\exp(2[(\eta 1-\eta)^2 + (\eta 2-\eta)^2 + (\eta 3 - \eta)^2]^{1/2})$, where $\eta 1 = \ln K1$, $\eta 2 = \ln K2$, $\eta 3 = \ln K3$, and $\eta = \ln (K1 + K2 + K3)^{1/3}$. A value of Pj =1 describes a perfectly isotropic fabric, a Pj value of 1.15 describes a sample with 15% anisotropy and so on. Following the above, Pj values of 0–5% indicate a weak anisotropy, 5–10% moderate anisotropy, 10– 20% a strong anisotropy, and >20% a very strong anisotropy. The shape of the susceptibility ellipsoid (T) (with $T = (2\ln k_2 - \ln k_1 - \ln k_3)/(\ln k1 - \ln k_3)$) (Jelinek, 1981) ranges from +1 where purely oblate to −1 where purely prolate, and is triaxial near zero. We measured the AMS of 305 specimens prepared from samples collected at 18 sites distributed across the Buena Vista intrusion (Table 2). All sample sites were precisely

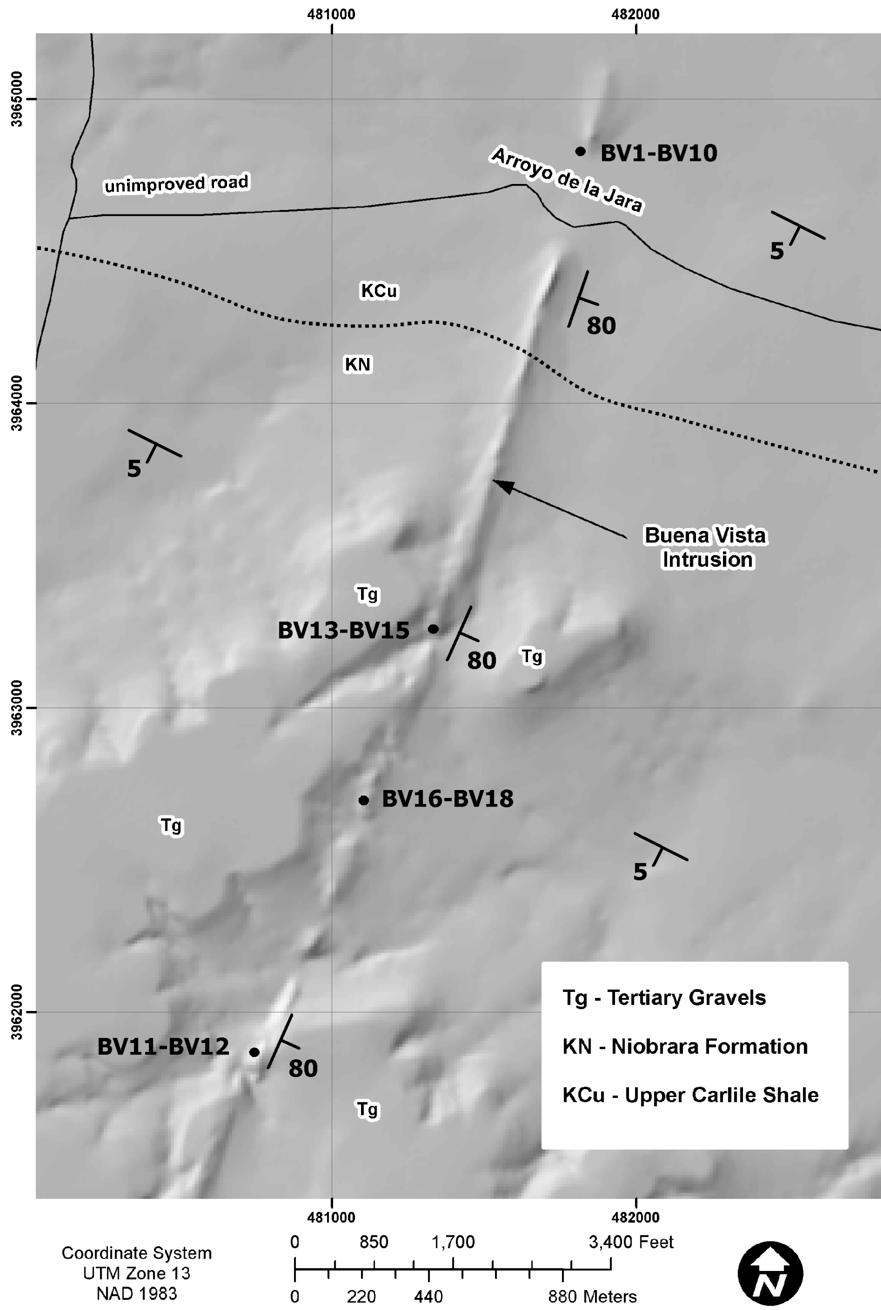

FIGURE 2. Digital elevation model of the Buena Vista intrusion showing the contact between the late Cretaceous Carlile Shale in the north with the Niobrara Formation to the south. Solid circles indicate paleomagnetic and anisotropy of magnetic susceptibility site locations. Four of the geochronology sites are located near BV1-BV10 and one site is located near BV11-BV12.

TABLE 1. Paleomagnetic data from the Buena Vista Intrusion

Site	Rock Type	n/N	R	Dec	Inc	α95	k	Lat VGP	Long VGP	Northing NAD1983	Easting Zone 13N
BV1	HG	8/9	7.84	**161.1**	**-73.2**	8.4	44.0	***-63.8***	***52.5***	3964819	481815
BV2	HG	4/9	3.94	**191.4**	**-47.8**	13.0	51.0	***-78.3***	***197.4***	3964818	481823
BV3	HG	8/10	7.95	**194.9**	**-59.1**	4.9	130.7	***-77.5***	***141.2***	3964815	481824
BV4	TA	7/10	6.80	**200.7**	**-60.6**	11.2	29.9	***-72.7***	***135.0***	3964822	481829
BV5	APB	7/8	6.99	**194.5**	**-57.8**	2.9	427.5	***-78.1***	***147.6***	3964824	481833
BV6	TA	6/9	5.97	**176.0**	**-77.1**	5.6	145.3	***-60.1***	***71.4***	3964844	481831
BV7	TA	4/8	3.91	**175.9**	**-77.7**	16.2	33.1	***-59.3***	***71.6***	3964844	481831
BV8	HG	reject								3964844	481831
BV9	HG	reject								3964854	481827
BV10*	HG	4/10	3.92	**226.6**	**-79.1**	15.5	36.3	***-48.3***	***97.9***	3964867	481831
BV11	HG	6/8	5.99	**205.4**	**-55.9**	3.0	492.7	***-69.5***	***155.5***	3961795	480728
BV12	HG	8/9	7.99	**196.9**	**-57.7**	2.4	535.3	***-76.3***	***149.1***	3961795	480728
BV13	HG	reject								3963236	481333
BV14	HG	8/8	7.97	**197.0**	**-55.0**	3.4	270.1	***-76.2***	***160.9***	3963224	481333
BV15	APB	8/11	7.96	**56.1**	**15.3**	4.3	166.7	***31.8***	***359.3***	3963236	481341
BV16	HG	reject								3962664	481108
BV17*	HG	3/8	2.99	**239.1**	**-12.2**	6.1	414.3	***28.5***	***178.7***	3962650	481100
BV18*	APB	6/9	5.92	**155.1**	**-49.5**	8.6	61.1	***-68.5***	***337.3***	3962634	481098
G-Mean	n=13	13/14	11.18	**196.9**	**-61.1**	11.2	14.7	***-75.4***	***133.8***		
G-Mean#	n=10	10/14	9.82	**192.9**	**-62.9**	6.9	55.4	***-77.2***	***121.3***		

Explanation: n/N - ratio of number of samples used to calculate the site mean to total number of samples collected at the site; R - resultant vector length, Dec/Inc - site mean declination and inclination; α_{95} - 95% confidence interval of the estimated site mean direction, assuming a circular distribution; k - best estimate of (Fisher) precision parameter; Lat/Long VGP—latitude and longitude of site mean virtual geomagnetic pole; UTM locations of all sites NAD 1983. Expected field direction: D=358.8°, I=58.3°, α_{95}= 5.0° (Besse and Courtillot, 2003). Augite porphyritic basalt (APB); hornblende-bearing gabbro (HG); tourmaline anorthosite (TA). *Sites were rejected as the mean was greater than 18 degrees of the overall group mean result. #accepted group mean.

positioned using a Garmin CSx60 GPS (WGS 84). AMS measurements were performed on an AGICO MFK1-A multi-function kappabridge operating at low alternating field of 200 A/m at 976 Hz at the New Mexico Highlands University Paleomagnetic-Rock Magnetism laboratory.

Rock Magnetism

To characterize the magnetic mineralogy, we conducted a suite of rock magnetic experiments with the principal goal of identifying the mineral phase(s) that carry the overall remanence, the AMS fabric, the quantity, composition, and grain size of the magnetic phase(s) present, and whether the materials carry a geologically stable remanence. Rock magnetic experiments included (1) analysis of low-field susceptibility versus temperature and (2) zero field (ZF) and applied field cooling (FC) and warming experiments 4 to 300 K. All susceptibility experiments were measured with an AGICO MFK1-A kappabridge susceptibility meter and the FC-ZFC experiments utilized a Quantum Design 7 Tesla magnetic properties measurement system (MPMS) system. Curie point estimates define the magnetic phase(s) present in the sample and provide insight into the magnetic domain state. The FC-ZFC experiments are used primarily for magnetic mineral identification based on low-temperature crystallographic transitions (e.g., the Verwey transition (Verwey, 1939)) and for characterizing particle size distributions.

$^{40}Ar/^{39}Ar$ Methods

$^{40}Ar/^{39}Ar$ age determinations were conducted on five samples representing discrete phases within the composite Buena Vista intrusion and one sample from the Read's Ranch. The samples were crushed using a mortar and pestle and 1 gram of amphibole crystals were picked using tweezers. The specimens were analyzed either as groundmass concentrates or amphibole crystals at the New Mexico Geochronological Research Laboratory at New Mexico Institute of Mining and Technology in Socorro, NM following the laboratory's standard procedures (see https://geoinfo.nmt.edu/labs/argon/methods/home.html).

RESULTS

General Demagnetization Behavior

Fourteen of the eighteen sample sites yield interpretable results (Table 1). The four sites that did not yield interpretable data had high dispersion between samples from the same site or did not yield stable end-point behavior; these sites are not discussed further. Overall, progressive alternating field (AF) and thermal demagnetization response is characterized by high quality results (Fig. 3) with a near linear trajectory to the origin defined over a broad range of peak fields and temperatures. Duplicate specimens treated with thermal demagnetization yield directional data similar to those resolved in AF demagnetization with

TABLE 2. Anisotropy of magnetic susceptibility data from the Buena Vista Intrusion

Site	Location	Rock Type	N	No	KM 10^{-3} SI	K1 Trend	Plunge	K2 Trend	Plunge	K3 Trend	Plunge	K1-K2 plane Strike/Dip	L	F	Pj	T	Shape
BV1	West	HG	18	18	322	195	15	38	74	286	6	016/84 E	1.019	1.050	1.071	0.451	O
BV3	East	HG	22	22	357	202	19	9	70	110	4	110/79 S	1.020	1.031	1.053	0.209	O
BV6	East	TA	17	17	101	201	29	16	61	110	2	200/88 W	1.005	1.038	1.048	0.768	O
BV7	West	TA	20	20	115	195	25	8	65	104	3	194/87 W	1.007	1.037	1.048	0.689	O
BV9	East	HG	18	18	375	8	9	260	62	102	26	192/64 W	1.002	1.008	1.011	0.534	O
BV10	West	HG	23	23	490	195	20	29	70	286	5	016/85 E	1.004	1.020	1.026	0.636	O
BV11	West	HG	15	15	361	148	82	29	4	298	7	028/83 E	1.005	1.105	1.125	0.903	O
BV12	East	HG	13	13	191	192	55	40	31	302	13	032/77 E	1.009	1.063	1.079	0.744	O
BV16*	East	HG	8	8	58.1	194	20	98	17	331	63	061/27 S	1.004	1.010	1.014	0.403	O
BV18*	East	HG	20	20	42.8	126	6	225	58	32	32	122/58 S	1.007	1.003	1.010	-0.402	P
BV17	West	HG	9	9	59.7	134	57	351	27	252	17	342/73 E	1.001	1.009	1.011	0.705	O
BV2	Center	HG	10	10	34	207	25	30	65	297	1	027/89 E	1.004	1.022	1.029	0.671	O
BV4	East	TA	24	24	370	5	33	212	54	104	13	194/77 W	1.003	1.021	1.026	0.767	O
BV5*	-	APB	17	17	136	271	18	169	31	26	53	116/37 S	1.001	1.002	1.003	0.264	P
BV8	Center	HG	21	21	478	207	38	6	50	109	11	199/79 W	1.006	1.028	1.036	0.642	O
BV13	Center	HG	16	16	278	193	34	32	55	289	9	019/81 E	1.006	1.093	1.112	0.882	O
BV14	Center	HG	12	12	53	27	64	190	25	283	7	013/83 E	1.006	1.048	1.060	0.773	O
BV15	-	APB	22	22	10.4	209	30	17	60	116	5	206/85 W	1.008	1.024	1.034	0.489	O

Explanation: Site, AMS sampling site; Location, dike margin; Rock Type, See Table 1; N, number of samples collected at each site, No, number of accepted specimens at each site, typically, one to three specimens per sample; Km, magnitude of susceptibility (in 10E-3 SI); K1, *in situ* trend and plunge (in degrees) of magnetic lineation; K2, *in situ* trend and plunge (in degrees) of the intermediate susceptibility; K3, *in situ* trend and plunge (in degrees) of normal to magnetic foliation plane; K1-K2 plane, strike and dip of the magnetic foliation plane; L, magnetic lineation ((K1-K2)/Km); F, magnetic foliation ((K2-K3)/Km); Pj, magnitude of the corrected degree of anisotropy (Jelinek, 1981); T, shape parameter (Jelinek, 1981). Shape: P, prolate shape, O, oblate shape. *denotes a site with an inverse AMS fabric.

thermal unblocking temperature spectra from 550°C to 630°C with most samples fully demagnetized by 580°C. Most samples contain a single characteristic remanent magnetization (ChRM) that is well-grouped at the site level, but some samples also contain additional magnetizations vectors that are readily randomized by 10 mT or by 250°C (Fig. 3). We interpret these magnetization components as low-coercivity viscous remanent magnetization overprints (VRM). After removing the VRM, the ChRM, which we interpret as the primary thermal remanent magnetization (TRM), decays along a roughly univectoral path to the origin with less than ten percent of the natural remanent magnetization (NRM) intensity remaining after treatment in 120 mT fields or by 580°C in most cases (Fig. 3).

Paleomagnetic Results

Paleomagnetic data from the fourteen accepted sites yield both normal (n=1) and reverse polarity (n=13) magnetization directions, which when the one normal polarity site is excluded, yields an overall group mean of declination (D) = 196.9°, inclination (I) = -61.1°, α95 = 11.2°, k = 15.9 (Fig. 4). Of the thirteen accepted sites, three are greater than 18° from the overall group mean and we consider these site means as outliers. Recalculating the group mean (n=10), yields a reverse polarity group mean direction of D = 192.9°, I = -62.9°, α95 = 6.9°, k = 55.4. This is clockwise discordant to the mid-Miocene reverse polarity expected field direction (D= 172.1°, I=-54.8°, α95= 2.7°), which is based on the 15 Ma synthetic paleomagnetic pole of Besse and Courtillot (2002) and has an inferred rotation (R) and a flattening (F) of R = 20.8° ±12.4° and F = -7.8° ±7.2° (Demarest, 1983; Fig. 4). The expected dispersion of the virtual geomagnetic poles (VGPs) for the latitude of north central New Mexico (35° N) is estimated at 15° (Merrill and McElhinny, 1983). Considering the thirteen sites that yield interpretable results, we estimate a VGP dispersion of 20.3° while the VGP dispersion of the ten accepted sites is 10.9°.

Anisotropy of Magnetic Susceptibility Results

Magnetic susceptibility data for all sites are summarized in Table 2 together with all principal magnetic parameters measured. Km intensities for the intrusions are high, ranging from 209 x 10^{-3} to 53 x 10^{-3} and with a mean of 212 x 10^{-3}. The AMS fabric results reveal an orderly pattern of K1 lineation and K1-K2 foliation plane data with susceptibility ellipsoids that are oblate (n=17) to prolate (n=1) (Table 2). The corrected degree of anisotropy (Pj; Jelinek, 1981) varies between 1.003 and 1.125, and averages 1.044, indicating a moderate to weak degree of anisotropy (Table 2). One site yields prolate shaped magnetic ellipsoids with the remaining sites yielding an oblate shaped magnetic ellipsoid shape. The magnetic lineation (L) and foliation (F) average 1.007 and 1.034 respectively. No correlation exists between Pj and Km or between the shape parameter (T) and the mean susceptibility.

AMS data from fifteen of the eighteen sites yield remarkably consistent results along the strike of the dike. Three sites

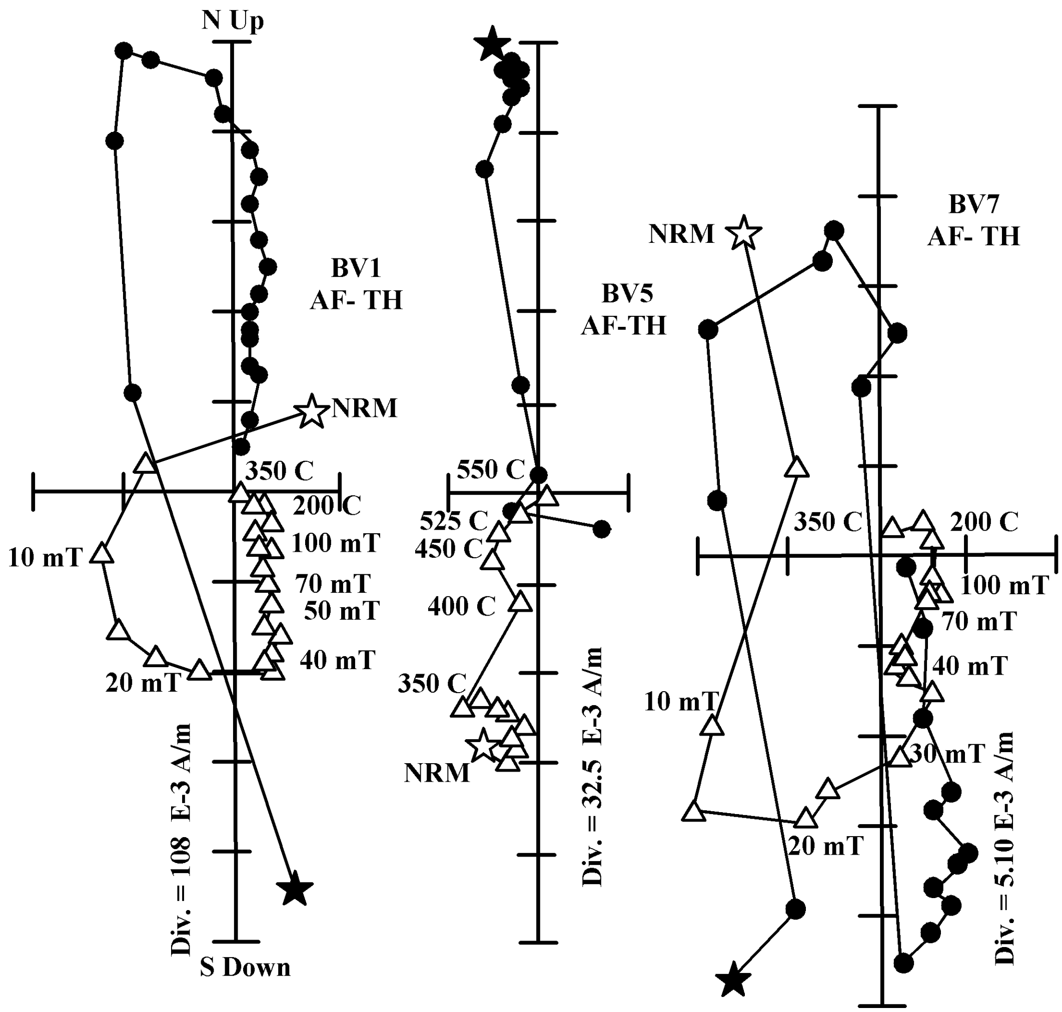

FIGURE 3. Representative *in situ* modified demagnetization diagrams (Zijderveld, 1967; Roy and Park, 1974) for rocks collected at the Buena Vista intrusion. Solid cirles represent the projection onto the horizontal plane, open triangles represent the projection on to the true vertical plane. Stars are the initial natural remanent magnetization prior to laboratory treatment. AF demagnetization steps are given in milliTesla (mT) and thermal demagnetization steps in degrees centigrade (C). Diagrams are designated by a site number (e.g., BV1), and method of treatment (AF or TH). Intensity (A/m) is shown along one axis for each sample, each div. equals indicated intensity.

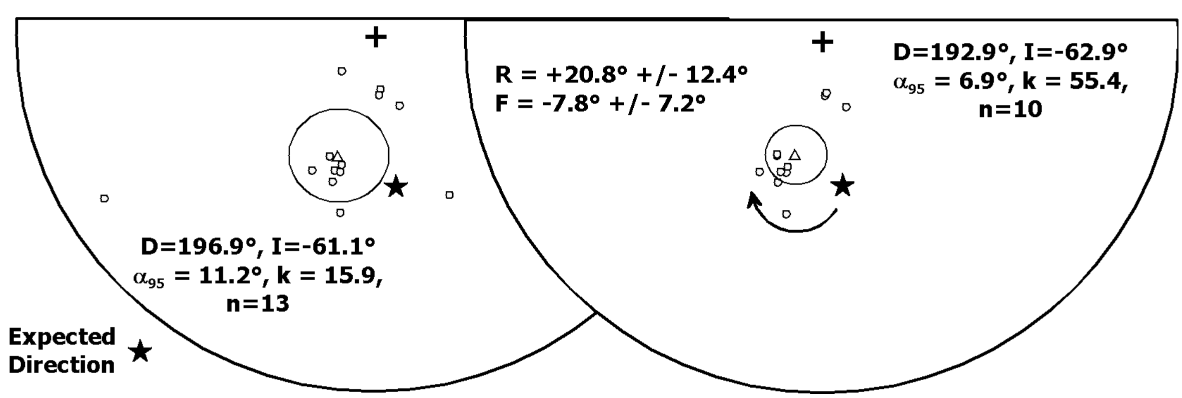

FIGURE 4. Lower hemisphere equal area projection of site mean paleomagnetic data. Diagram on the left shows all 13 accepted site mean directions (open circles), with associated group mean direction (open triangle), and confidence ellipse. Diagram on the right depicts the 10 accepted sites means used to calculate the group mean for the Buena Vista intrusion. Arrow indicates a clockwise vertical axis rotations relative to the mid Miocene expected field direction (Solid black star). D/I - site mean declination and inclination; α95–95% confidence interval of the estimated group mean direction, assuming a circular distribution; k - best estimate of (Fisher) precision parameter; n - number of sites used to calculate the group mean direction; R, rotation with respect to the expected direction with associated error; F, flattening with respect to the expected direction with associated error.

yield poorly defined susceptibility ellipsoids in which the K1 and K3 axes are switched. The high dispersion likely stems from hydrothermal alteration which resulted in the growth a very fine-grained, single domain titanomagnetic phase. Based on the AMS fabric data, these sites display an inverse fabric and evidence of remagnetization. The remaining fifteen sites yield well-defined oblate susceptibility ellipsoids with magnetic foliation planes that strike parallel to the trend of the dike (average strike and dip: 15°, 80°E). In thirteen of the fifteen sites, the K1 magnetic lineation trends south-southwest with a low plunge (<30°) and the magnetic foliation plane (K1-K2 plane) strikes north-northeast and dips steeply to the east and west (Fig. 5). At eleven sites, it was possible to sample the intrusion from paired dike margins allowing a unique flow direction to be defined. Three of the paired margin sites yield sub-horizontal flow directions that trend to the south-southwest and one set of paired margin sites yields steep downward flow to the southwest (Fig. 6). The other paired margin site (defined by three site means) did not yield interpretable results as two of the sites yield an inverse fabric. For the remaining seven sites, one site yields an inverse fabric, two sites yield K1 lineations that trend to the north, and the remaining four sites yield K1 lineations that trend to the south-southwest.

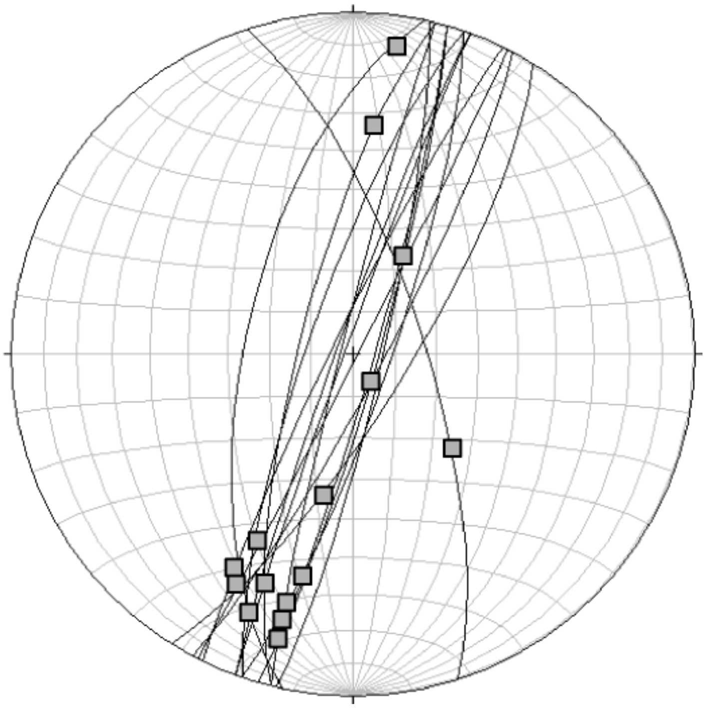

FIGURE 5. Lower hemisphere equal area projection of anisotropy of magnetic susceptibility data. The grey squares are the K1 magnetic lineation direction. The great circles are the strike and dip of the magnetic foliation plane defined by the K1-K2 axes. The strike/dip of the Buena Vista intrusion is roughly 015°E, 80°SE. The magnetic foliation plane parallels the overall strike of the intrusion.

Rock Magnetic Results

The Curie point estimates reveal two temperature intervals using the Hopkinson peak (Hopkinson, 1890) or inflection point methods (Tauxe, 1998); one from 300ºC to 350ºC and another from 520ºC to 565ºC. The Curie point estimates between 300°C to 350°C likely reflect the contribution of pyrrhotite or coarse grained maghemite while the higher temperature interval suggest a limited range of moderate to low Ti titanomagnetite compositions (Dunlop and Özdemir, 1997). None of the samples analyzed show a sharp Hopkinson peak that would be indicative of single domain magnetite; rather most samples show a distributed peak over tens of degrees Celsius followed by a rapid drop in susceptibility at the Curie point. We interpret this behavior to reflect the presence of pseudosingle to multidomain titanomagnetite. The low temperature MPMS experiments reveal similar behavior between four of the six samples analyzed with a sharp loss in remanence over the temperature interval of 130 K to 120 K. This temperature interval is a diagnostic crystallographic phase transition indicating the presence of a unique ferromagnetic

TABLE 3: $^{40}Ar/^{39}Ar$ from the Buena Vista Intrusion and Read's Ranch Stock

		UTM NAD 83					
Sample	**Mineral**	**Easting (m)**	**Northing (m)**	**Elevation(m)**	**Age (Ma) +/- error**	**Age**	**Comments**
hornblende gabbro							
BVD-1	Hbd	3964813	481818	2089	*14.62 +/- 0.04	14.61 +/- 0.04	Weighted Mean
BVD-5	GC	3964846	481836	2100	*14.62 +/- 0.04	14.63 +/- 0.07	Weighted Mean
tourmaline anorthosite							
BVD-2	Hbd	3964835	481836	2099	-	#19.15 +/- 0.70	Rejected
olivine basalt							
BVD-3	GC	3961787	480736	2156	*14.71 +/- 0.06	14.87 +/- 0.31	Weighted Mean
BVD-4	GC	3964824	481836	2097	14.82 +/- 0.03	*14.20 +/- 0.14	Isochron
Reads Ranch Stock							
BVD-6	Hbd	3937046	486065	2050	14.92 +/- 0.03	*14.87 +/- 0.07	Isochron

Explanation: *preferred age; #disturbed age spectrum; Hbd, hornblende; GC, groundmass concentrate.

Sample preparation and irradiation: Minerals separated with standard heavy liquid, Franz Magnetic and hand-picking techniques. Samples in NM-272 irradiated in a machined Aluminum tray for 8 hours in C.T. position, USGS TRIGA, Denver, Colorado. Neutron flux monitor Fish Canyon Tuff sanidine (FC-2). Assigned age = 28.201 Ma (Kuiper et al., 2008).

Instrumentation: Total fusion monitor analyses performed on an Argus VI mass spectrometer on line with automated all-metal extraction system. System = Jan. Step-heat analyses performed on a Argus VI mass spectrometer on line with automated all-metal extraction system. System = Obama. Multi-collector configuration: ^{40}Ar-H1, ^{39}Ar-Ax, ^{38}Ar-L1, ^{37}Ar-L2, ^{36}Ar-CDD. Flux monitors fused with a Photon Machines Inc. CO_2 laser. Groundmass concentrate and hornblende step-heated with a Photon Machine Inc. Diode laser.

Analytical parameters: Sensitivity for the Argus VI with the Diode laser (step-heated samples) is 9.84e-17 moles/fA. Sensitivity for the Argus VI with the CO_2 laser (fused monitors)is 4.62 e-17 moles/fA. Typical system blank and background was 194, 1.76, 0.197, 4.92, 0.59 x 10^{-18} moles at masses 40, 39, 38, 37 and 36, respectively for the laser analyses. J-factors determined by CO_2 laser-fusion of 6 single crystals from each of 8 radial positions around the irradiation tray. Decay constants and isotopic abundances after Min et al. (2000).

phase, in this case, low oxidation state titanomagnetite (Verwey, 1939). On cooling, the remanence remains constant up to ~130 K and falls off rapidly from 130 K to 120 K and remains approximately constant to 10 K. The large initial remanence on the warming curve is the low temperature saturation isothermal remanent magnetization (LTSIRM) and does not reflect any paramagnetic component. The sharp drop between 120 K and 130 K further confirms the presence of titanomagnetite. Two samples (olivine basalt and tourmaline anorthosite) display a sharp drop in remanence on warming between 10 K to 50 K that may be due to the pyrrhotite transition or to some other unknown phase that disorders or unblocks below 50 K. In summary, the rock magnetic data and demagnetization behavior (Fig. 3) indicate that the dominant magnetic phase is cubic Fe-Ti oxide of a restricted magnetic grain size between pseudosingle to multidomain titanomagnetite.

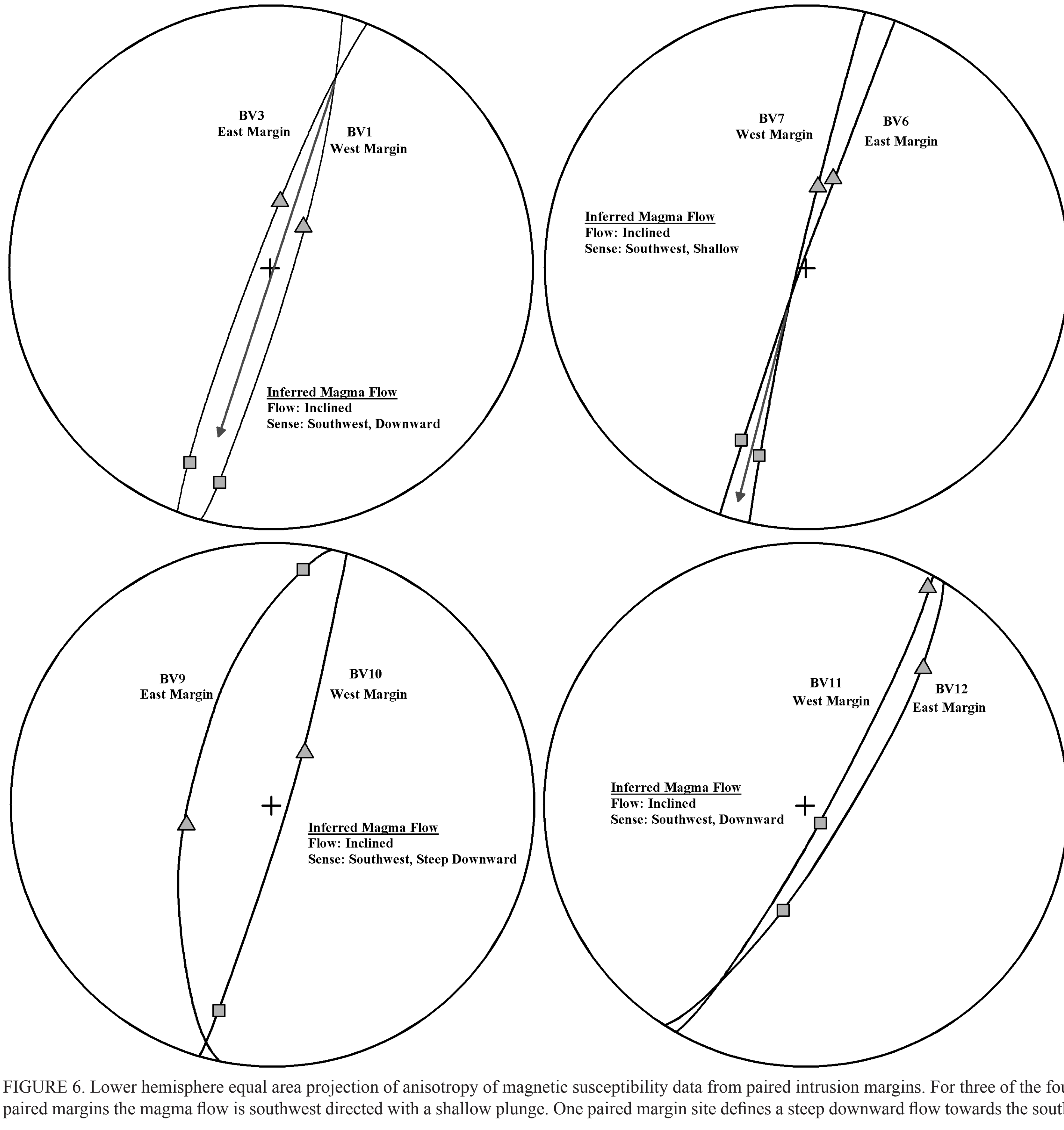

FIGURE 6. Lower hemisphere equal area projection of anisotropy of magnetic susceptibility data from paired intrusion margins. For three of the four paired margins the magma flow is southwest directed with a shallow plunge. One paired margin site defines a steep downward flow towards the south.

$^{40}Ar/^{39}Ar$ Results

Five samples from the Buena Vista intrusion were dated using the $^{40}Ar/^{39}Ar$ technique on hornblende separates or groundmass concentrates (Table 3) with two dates from the main phase hornblende gabbro, one date from the central tourmaline anorthosite, and two dates from olivine porphyritic basalt. The data from the two hornblende gabbro sites yield indistinguishable ages of 14.62 ±0.02 Ma. The one sample from the tourmaline anorthosite yields a disturbed age spectra and we did not assign this sample an age. One sample of the olivine basalt collected from Arroyo de la Jara had excess Ar ($^{40}Ar/^{36}Ar$ ratio of 340 ±6) and yielded an isochron age of 14.20 ±0.14 Ma and a plateau age that contains ~51% of the 39 gas of 14.87 ±0.43 Ma with MSWD of 3.6; we assigned the isochron age to this sample. The other olivine basalt sample, collected from the southern part of the intrusion, yields

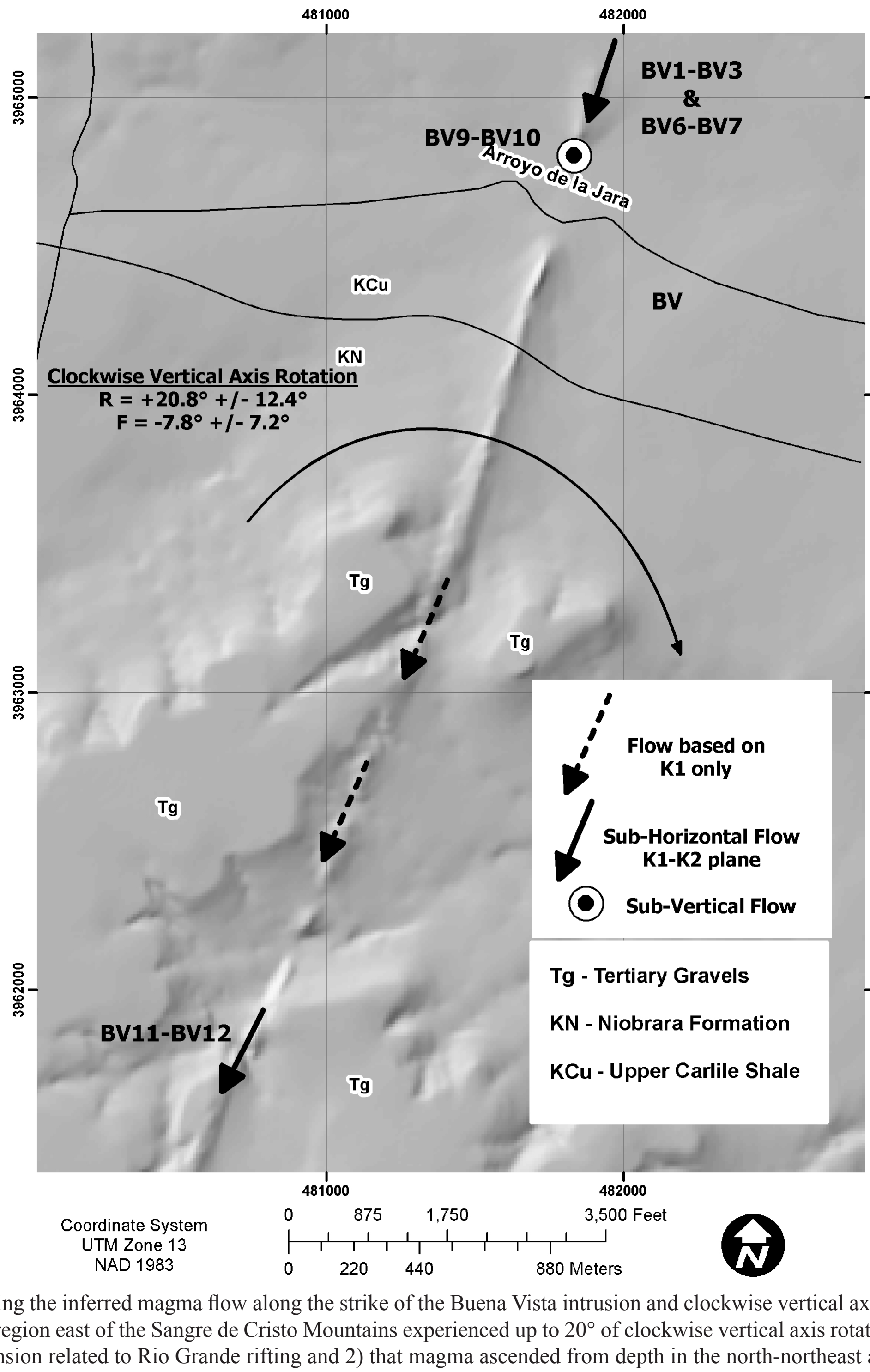

FIGURE 7. Map depicting the inferred magma flow along the strike of the Buena Vista intrusion and clockwise vertical axis rotation of the region. We hypothesize 1) that the region east of the Sangre de Cristo Mountains experienced up to 20° of clockwise vertical axis rotation post mid-Miocene associated with crustal extension related to Rio Grande rifting and 2) that magma ascended from depth in the north-northeast and flowed sub-horizontally to the south-southwest at a shallow depth. Pervasive miarolitic cavities throughout the intrusion argue for a shallow level of emplacement.

a well-defined plateau age of 14.71 ±0.06 Ma. A sixth sample from a gabbro stock located just east of Las Vegas yields a well-defined isochron age of 14.87 ±0.07 Ma. Based on the new $^{40}Ar/^{39}Ar$ data, magmatic activity in the Las Vegas area spanned roughly 600 ka.

DISCUSSION

Paleomagnetic Implications for Tectonic Deformation

Table 1 summarizes the paleomagnetic results from the sites sampled at the Buena Vista intrusion. Several factors may influence the observed remanence direction from a given intrusion, such as the age of the magnetization, overprinting secondary magnetization because of chemical alteration and/or remagnetization, and tectonic disturbance. Given the somewhat low VGP dispersion estimate (s=10.9°; n=10) of the group mean, relative to the expected VGP dispersion estimate (s=15°), it is possible that the Buena Vista intrusion was emplaced quickly relative to secular variation. However, the new $^{40}Ar/^{39}Ar$ age determinations constrain the age of emplacement to more than half a million years (Table 3), more than adequate to average secular variation of Earth's magnetic field (Irving and Pullaiah, 1976). Remagnetization does not appear to explain adequately the remanence directions as the intrusion yields a simple demagnetization behavior with no evidence, at the outcrop, thin section, or in rock magnetic character of any pervasive alteration or secondary magnetization components. We therefore attribute the statistically distinct, clockwise discordant remanence direction, with respect to the middle Miocene expected magnetic field direction, to reflect a post-emplacement tectonic disturbance of the intrusion.

The brittle crust deforms by displacement, distortion, and rigid-body rotation. In the western Great Basin, parts have been considerably modified by the well-recognized system of right-lateral faults defining the Walker Lane in response to different phases of Neogene deformation (Petronis et al., 2012). In this region, a considerable amount of crustal vertical-axis rotation has occurred and accommodated a substantial amount of the cumulative strain. Rigid-body rotations about a vertical axis are not always straightforward to identify, quantify, and explain, despite the fact that they can be a major contributor to finite strain. Paleomagnetic analysis of appropriate materials has proven to be a powerful technique for detecting and quantifying such rotations. Numerous paleomagnetic studies have documented variable degrees (or lack thereof) of vertical-axis rotation associated with strike-slip faulting and extension (e.g., Gillett and Van Alstine, 1982; Ron et al., 1984; Hudson and Geissman, 1987, 1991; Janecke et al., 1991; Hudson et al., 1994; Wawrzyniec et al., 2002; Petronis et al., 2002; Hudson, 1992; Cashman and Fontaine, 2000; Petronis et al., 2007; Petronis et al., 2012). To our knowledge, no studies east of the Sangre de Cristo Mountains at the latitude of Las Vegas, NM have documented rigid-body rotation about a vertical axis associated with crustal extension. We argue that the Buena Vista intrusion and the associated region east of the front range of the Sangre de Cristo Mountains have experienced modest clockwise vertical axis rotation, post mid-Miocene, likely associated with crustal extension related to Rio Grande rifting (Figs. 4, 7). As the crust deforms under extension, if the displacement vector is oblique to the dip of the fault plane, it is often possible for fault bounded crustal blocks to accommodate strain via vertical axis rotation.

Implications of the AMS data

Common models of dike emplacement envision the magma feeder as a conduit transporting molten rock from a reservoir to the emplacement level often controlled by a neutral buoyancy level between magma pressure and lithostatic load. To reveal the controls on the development of dikes, Geshi et al. (2012a, 2012b) investigated numerous intrusions exposed on the 400-m-high cliff of the Miyakejima Caldera (Japan). Their results show that the magmatic overpressure and mechanical properties of the host rock control the entire structure of dikes. Dike thicknesses increase with altitude, reflecting changes in the mechanical properties of the rocks surrounding the dikes and the gradient of the magmatic overpressure inside the dikes. When a dike reaches the ground surface and erupts, dike thickness decreases with the drop of magmatic overpressure inside the dike. Geshi et al.'s (2012a) results, as well as many other studies (e.g., Gudmundsson et al., 2008; Geshi et al., 2010, 2012b; Galindo and Gudmundsson, 2012) suggest that careful and detailed observation of ground deformation by dike intrusion can reveal the change of magmatic overpressure within a dike. These observations are consistent with other studies that suggest magmas migrate laterally with control by pre-existing subhorizontal structures and studies that have documented lateral flow of shallow igneous bodies at a considerable horizontal distance (>20 km) from their ascent area (Mackin, 1947; Van Kooten, 1988; Staudigel et al., 1992; Varga et al., 1998; Abelson et al., 2001; Poland et al., 2004; Petronis et al., 2004; Magee 2011; Petronis et al., 2013).

The low-field AMS technique can detect submicroscopic mineral alignments and is an excellent tool for rapid, accurate measurement of petrofabrics and, to a certain extent, provides an estimate of the amount of strain (Borradaile and Henry, 1997; Bouchez, 1997, 2000). Even in weakly anisotropic material, it is now generally accepted (Bouchez, 1997) that the magnetic lineation and foliation plane reflect the magmatic fabric and can provide information on magma migration and flow direction and/or sense (Hrouda, 1982; Rochette et al., 1992; Tauxe et al., 1998). As outlined by many researchers, AMS reflects the statistical alignment or anisotropy of the magnetic phases and reflects or mimics the petrofabric of the material (Khan, 1962, Taira and Lienert, 1979; Hargraves et al., 1991; Varga et al., 1998). Knight and Walker (1988) first described the empirical relationship between outcrop flow indicators and AMS defining its use as a proxy flow indicator and numerous others have since expanded this work (Benn and Allard, 1989; Rochette et al., 1991; Rochette et al., 1992; Tauxe et al., 1998; Varga et al., 1998; Aubourg et al., 2002; Bervera et al., 2001; Callot et al., 2001; Geoffroy et al., 2002; Poland et al., 2004; Warwick et al., 2011). During emplacement of sheet intrusions elongate phenocrysts can become imbricated against the chilled margins due to simple shear and, since oxides are often late stage crystallization products, they may also be distributed to mimic the preexisting silicate fabric (Hargraves et al., 1991; Stephenson, 1994). In an ideal case, AMS fabrics from the two margins of the dike are distinct and plot on either side of the dike trace on a stereographic projection defining a flow direction and the sense of magma flow, i.e. the magma flow vector (Staudigel et al., 1992; Varga et al., 1998; Geoffroy et al., 2002; Callot et al., 2001). The orientation of the K1-K2 planes along each margin can be used to infer the flow vector. Essentially, in cross section across the dike, the paired margins fabric K1 lineations or K1-K2 planes form a "V" pattern that closes in the sense of flow (e.g., V = downward flow; Λ = upward flow) (see Tauxe et al., 1998; Callot et al., 2001; Geoffroy et al., 2002). Based on the AMS data from the Buena Vista intrusion, we argue that magma rose from depth until reaching a neutral buoyancy level and then flowed horizontally from the north-northeast to the south-southwest (Fig. 7).

CONCLUSIONS

Based on the results from the Buena Vista intrusion we reach the following conclusions. The paleomagnetic data are discordant to the Middle Miocene expected field direction with an inferred rotation and flattening of R = 20.8° ±12.4° and F = -7.8° ±7.2°. We attribute the discordant paleomagnetic data to indicate the region east of the Sangre de Cristo Mountains at the latitude of the study area experienced statistically distinct clockwise vertical axis rotation associated with Rio Grande rift extensional tectonism. Four of five $^{40}Ar/^{39}Ar$ age determinations constrain magmatic activity in the Las Vegas igneous province between 14.20 Ma to 14.87 Ma. The AMS data from fifteen sites yield internally consistent results and data from four paired dike margins define a magmatic flow direction from the north-northeast to the south-southwest. The comparison between structural observations, paleomagnetic, and AMS data show that these methods provide valuable complementary data on dike propagation and subsequent magma flow within intrusions. The results of this study demonstrate collectively that shallow-level intrusions can be internally complex. Therefore, the processes described at the Buena Vista intrusion can have a more general application as an analog of large strike length intrusions worldwide and beyond.

ACKNOWLEDGMENTS

Funding for this project was awarded by American Association of Petroleum Geologists, Rocky Mountain Association of Geologists, New Mexico Geological Society, Natural Resources Career Track (NRCT)—USDA, and Sigma XI. A special thanks to Marvin Mascarenas, Carlos Martinez, Chick Bernie, the Buena Vista Ranch, Edward Martinez, and numerous NMHU geology students. We would like to thank Craig Magee (Imperial College London, UK), Brian O'Driscoll (University of Manchester, UK) and Carl T. Stevenson (University of Birmingham, UK) for constructive reviews of the manuscript.

REFERENCES

Abelson, M., Baer, G., and Agnon, A., 2001, Evidence from gabbro of the Troodos ophiolite for lateral magma transport along a slowspreading mid-ocean ridge: Nature, v. 409, p. 72–75.

Aubourg, C., Giordano, G., Mattei, M., and Speranza, F., 2002, Magma flow in sub-aqueous rhyolitic dikes inferred from magnetic fabric analysis (Ponza Island, W. Italy): Physics and Chemistry of the Earth, v. 27, p. 1263–1272.

Benn, K. and Allard, B., 1989, Preferred mineral orientations related to magnetic fabric in ophiolite layered gabbros: Tectonophysics, v. 233, p. 153–162.

Bervera, E., Walker, G.P.L., Canon-Tapia, E., and Garcia M.O., 2001, Magnetic fabric and inferred flow direction of dikes, conesheets and sill swarms, Isle of Skye, Scotland: Journal of Volcanology and Geothermal Research, v. 106, p. 195–210.

Besse, J., and Courtillot, V., 2002, Apparent and true polar wander and the geometry of the geomagnetic field over the last 200 Myr (v. 107, art no. 2300, 2002): Journal of Geophysical Research, v. 108, p. 2469, doi: 10.1029/2000JB000050.

Borradaile, G.J. and Henry, B., 1997, Tectonic applications of magnetic susceptibility and its anisotropy: Earth Science Reviews, v. 42, p. 49–93.

Bouchez, J.L., 1997, Granite is never isotropic: an introduction to AMS studies of granitic rocks, *in* Bouchez, J.L., Hutton, D.H.W., Stephens, W.E. (eds), Granite: from segregation of melt to emplacement fabrics: Kluwer, Dordrecht, p. 96–112.

Bouchez, J., 2000, Magnetic susceptibility anisotropy and fabrics in granites: Comptes Rendus de l'Académie des Science: Paris 330, p. 1–14.

Callot, J.P., Geoffroy, L., Aubourg, C., Pozzi, J.P., and Mege, D., 2001, Magma flow of shallow dikes from the East Greenland volcanic margin inferred from magnetic studies: Tectonophysics, v. 335, p. 313–329.

Cashman, P.H., and Fontaine, S.A., 2000, Strain partitioning in the northern Walker Lane, western Nevada and north-eastern California: Tectonophysics, v. 326, p. 111–130, doi: 10.1016/S0040-1951(00)00149-9.

Demarest, H.H., 1983, Error analysis for the determination of tectonic rotations from paleomagnetic data, Journal of Geophysical Research, v. 88, p. 4321–4328.

Dunlop, D.J. and Özdemir, O., 1997, Rock magnetism: fundamentals and frontiers, Cambridge studies in magnetism, 3: New York, Cambridge University Press, 573 p.

Galindo, I. and Gudmundsson, A., 2012, Basaltic feeder dykes in rift zones: geometry, emplacement, and effusion rates. Natural Hazards and Earth System Sciences, v. 12, p. 3683–3700.

Geoffroy, P., Callot, J.P., Aubourg, C., and Moreira, M., 2002, Magnetic and plagioclase linear fabric discrepancy in dikes: a new way to define the flow vector using magnetic foliation: Terra Nova, p. 183–190.

Geshi, N., Kusumoto, S., and Gudmundsson, A., 2012a, Geometric difference between non-feeder and feeder dikes: Geological Survey of Japan, AIST (National Institute of Advanced Industrial Science and Technology), 1-1-1 Higashi, Tsukuba, Ibaraki 305–8567, Japan, p. 195–198.

Geshi, N., Kusumoto, S., and Gudmundsson, A., 2012b, Effects of mechanical layering of host rocks on dike growth and arrest: Journal of Volcanolology and Geothermal Research, v. 223–224, p. 74–82.

Geshi, N., Kusumoto, S., and Gudmundsson, A., 2010, Geometric difference between non-feeder and feeder dikes: Geology, v. 38, p. 195–198.

Gillett, S.L., and Van Alstine, D.R., 1982, Remagnetization and tectonic rotation of the upper Precambrian and lower Paleozoic strata from the Desert Range, southern Nevada: Journal of Geophysical Research, v. 87, p. 10,929–10,953, doi: 10.1029/JB087iB13p10929.

Gudmundsson, A., Friese, N., Galindo, I., and Philipp Sonja, L., 2008, Effects of mechanical layering of host rocks on dike growth and arrest: Geology, v. 36, p. 123–126, No. 2, 02.2008.

Hargraves, R.B., Johnson, D., and Chan, C.Y., 1991, Distribution anisotropy: the cause of AMS in igneous rocks?: Geophys Research Letters, v. 18, p. 2193–2196.

Hopkinson, J., 1890, Magnetic Properties of Alloys of Nickel and Iron: Proceedings of the Royal Society of London, v. 48, p. 1–13, doi:10.1098/rspl.1890.0001.

Hrouda, F., 1982, Magnetic anisotropy of rocks and its applications in geology and geophysics: Surveys in Geophysics, v. 5, p. 38–82.

Hudson, M.R., and Geissman, J.W., 1987, Paleomagnetic and structural evidence for middle Tertiary counterclockwise rotation in the Dixie Valley region, west-central Nevada: Geology, v. 15, p. 638–642, doi: 10.1130/0091–7613(1987)15<638:PASEFM>2.0.CO;2.

Hudson, M.R., and Geissman, J.W., 1991, Paleomagnetic evidence for the age and extent of middle Tertiary counterclockwise rotation, Dixie Valley region, west central Nevada: Journal of Geophysical Research, v. 96, p. 3979–4006, doi: 10.1029/90JB02424.

Hudson, M.R., Sawyer, D.A., and Warren, R.G., 1994, Paleomagnetism and rotation constraints for the middle Miocene southwestern Nevada volcanic field: Tectonics, v. 13, p.258–277, doi: 10.1029/93TC03189.

Hudson, M.R., 1992, Paleomagnetic data bearing on the origin of arcuate structures in the French Peak-Massachusetts Mountain area of southern Nevada: Geological Society of America Bulletin, v. 104, p. 581–594, doi: 10.1130/0016–7606(1992)104<0581:PDBOTO>2.3.CO;2.

Irving, E. and G. Pullaiah, 1976, Reversals of the geomagnetic field, magnetostratigraphy, and relative magnitude of paleosecular variation in the Phanerozoic: Earth Sci. Rev., v. 12, p. 35–64.

Janecke, S.U., Geissman, J.W., and Bruhn, R.L., 1991, Localized rotation during Paleogene extension in east central Idaho: Paleomagnetic and Geologic Evidence: Tectonics, v. 10, p. 403–432, doi: 10.1029/90TC02465.

Jelinek, V., 1981, Characterization of the magnetic fabric of rocks: Tectonophysics, v. 79, p. 63–70.

Khan, M.A., 1962, The anisotropy of magnetic susceptibility of some igneous and metamorphic rocks: Journal of Geophysical Research, v. 67, p. 2867–2875.

Kirschvink, J.L., 1980, The least-square line and plane and the analysis of paleomagnetic data: Geophysical Journal of the Royal Astronomical Society, v.62, p. 699–718.

Knight, M.D. and Walker, G.P.L., 1988, Magma flow directions in dikes of the Koolau complex, Oahu, determined from magnetic fabric studies: Journal of Geophysical Research, v.93, p .4301–4309.

Kuiper, K.F., Deino, A., Hilgen, F.J., Krijgsman, W., Renne, P.R., Wijbrans, J.R., 2008, Synchronizing Rock Clocks of Earth History: Science, v. 320, p. 500–504, doi: 10.1126/science.1154339.

Mackin, J.H., 1947, Some structural features of the intrusions in the Iron Springs district [Utah]: Utah Geological Society: Guidebook to the geology of Utah 2, 62 p.

MaGee, C., 2011, Emplacement of sub-volcanic cone sheet intrusion. Ph.D. thesis, Birmingham University, UK, p. 243

Merrill, R.T. and McElhinny, M.W., 1983, The Earth's magnetic field: Academic: London, 401 p.

Min, K., Mundil, R., Renne, P.R., Ludwig, K.R., 2000, A test for systematic errors in 40Ar-39Ar geochronology through comparison with U-Pb analysis of a 1.1 Ga rhyolite. Geochimica Cosmochimica Acta, v. 64, p. 73–98.

Olmstead, B.W. and McIntosh, W.C., 2004, $^{40}Ar/^{39}Ar$ geochronology of the Ocate volcanic field, north central New Mexico: New Mexico Bureau of Geology & Mineral Resources Bulletin, v.160, p. 297–308.

Petronis, M.S., Geissman, J.W., Oldow, J.S., and McIntosh, W.C., 2002, Paleomagnetic and $^{40}Ar/^{39}Ar$ geochronologic data bearing on the structural evolution of the Silver Peak extensional complex, west-central Nevada: Geological Society of America Bulletin, v.114, no.9, p. 1108–1130.

Petronis, M.S., Hacker, D.B., Holm, D.K., Geissman, J.W., and Harlan, S.S., 2004, Magmatic flow paths and paleomagnetism of theMiocene Stoddard Mountain Laccolith, iron axis region, southwest Utah, USA: *in* Martin-Hernandez, F., Luneburg, C.M., Aubourg, C. Jackso, M. (eds) Magnetic fabric: methods and applications. The Geological Society of London Special Publications, v. 238, p. 251–283.

Petronis, M.S., Geissman, J.W., Oldow, J.S., and McIntosh, W.C., 2007, Tectonism of the southern Silver Peak Range: Paleomagnetic and geochronologic data bearing on the Neogene development of a regional extensional complex, central Walker Lane, Nevada: *in* Roeske, S., Till, A., Foster, D., and Sample, J., eds., Exhumation Associated with Continental Strike-Slip Fault Systems: Geological Society of America Special Paper 434, p. 81–106.

Petronis, M.S., O'Driscoll, B., Stevenson, C.T.E, and Reavy, R.J., 2012, Regional structural controls on the emplacement of the Ross of Mull Granite, NW Scotland, Geological Society of American Bulletin, doi: 10.1130/B30362.1, v. 124 no. 5–6 p. 906–927.

Petronis, M.S., Delcamp, A., van Wyk de Vries, B., 2013, Magma emplacement in the Lemptegy scoria cone (Chaine Des Puys, France) explored with structural anisotropy of magnetic susceptibility, and Paleomagnetic data. Bulletin of Volcanology, v.75, p. 753.

Poland, M.P., Fink, J.H., and Tauxe, L., 2004, Patterns of magma flow in segmented silicic dikes at Summer Coon volcano, Colorado: AMS and thin section analysis, Earth and Planetary Science Letters, v.219, p.155–169.

Rochette, P., Jenatton, L., Dupuy, C., Boudier, F., and Reuber, I., 1991, Diabase dike emplacements in Oman ophiolite a magnetic fabric study with reference to the geochemistry: *in* Ophiolite Genesis and Evolution of the Oceanic Lithosphere (ed) . Kluwer, Dordrecht, p. 55–82.

Rochette, P., Jackson, M., and Aubourg, C., 1992, Rock magnetism and the interpretation of ansisotropy of magnetic susceptibility: Reviews of Geophysics, v. 30, p. 209–226.

Ron, H., Freund, R., Garfunkel, Z., and Nur, A., 1984, Block rotation by strike slip faulting: Structural and paleomagnetic evidence: Journal of Geophysical Research, v.89, p. 6256–6270, doi: 10.1029/JB089iB07p06256.

Roy, J.L. and Park, J.K., 1974, The magnetization process of certain red beds: Vector analysis of chemical and thermal results: Canadian Journal of Earth Sciences II, p. 437–471.

Staudigel, H., Gee, J., Tauxe, L., and Varga, R., 1992, Shallow intrusive directions of sheeted dikes in the Troodos ophiolite: anisotropy of magnetic susceptibility and structural data: Geology, v.20, p. 841–844.

Stephenson, A., 1994, Distribution anisotropy: two simple models for magnetic lineation and foliation: Physics of the Earth and Planetary Interiors, v.25, p. 49–53.

Taira, A., and Lienert, B.R., 1979, The comparative reliability of magnetic, photometric and microscope methods of determining the orientations of sedimentary grains: Journal of Sedimentary Petrology, v. 49. p. 759–772.

Tarling, D.H., Hrouda, F., 1993, The magnetic anisotropy of rocks. Chapman and Hall, London, 217 p.

Tauxe, L., Gee, J.S., and Staudigel, H., 1998, Flow direction from anisotropy of magnetic susceptibility data: the bootstrap way: Journal of Geophysical Research, v.103, p. 17775–17790.

Tauxe, L., 1998, Paleomagnetic principles and practice, vol. 17 of modern approaches in geophysics:Kluwer, Dordrecht, 299 p.

Van Kooten, G.K., 1988, Structure and hydrocarbon potential beneath the Iron Springs laccolith, southwestern Utah:Geological Society of American Bulletin, v.100, p. 533–1540.

Varga, R.J., Gee, J.S., Staudigel, H., and Tauxe, L., 1998, Dike surface lineations as magma flow indicators within the sheeted dike complex of the Troodos ophiolite, Cyprus: Journal of Geophysical Research, v.10, p. 5241–5256.

Verwey, E. J., 1939, Electronic conduction of magnetite (Fe3O4) and its transition point at low temperature: Nature, v.144, p. 327–328.

Warwick, W., Hastie, P., Aubourg, C., and Watkeys, M.K., 2011, When an 'inverse' fabric is not inverse: an integrated AMS-SPO study in MORB-like dikes: Terra Nova, v. 23, p. 49–55.

Wawrzyniec, T.F., Geissman, J.W., Melker, M.D., and Hubbard, M., 2002, Dextral shear along the eastern margin of the Colorado Plateau: A kinematic link between Laramide contraction and Rio Grande rifting (ca. 75–13 Ma): The Journal of Geology, v.110, p. 305–324, doi: 10.1086/339534.

Zijderveld, J.D.A., 1967, A.C. demagnetization of rocks: analysis of results; *in* Collinson D.W., Creer K.M. and Runcorn S.K. (eds), Methods in Paleomagnetism: Elsevier, Amsterdam, p. 254–286.